Interaction between a Cationic Surfactant-like Peptide and Lipid Vesicles and Its Relationship to Antimicrobial Activity

Ashkan Dehsorkhi, Valeria Castelletto, and Ian W. Hamley*

School of Chemistry, Pharmacy and Food Biosciences, University of Reading, Whiteknights, Reading, RG6 6AD, United Kingdom

Jani Seitsonen and Janne Ruokolainen

Department of Applied Physics, Aalto University School of Science, P.O. Box 15100, FI-00076 Aalto, Finland

S *Supporting Information*

ABSTRACT: We investigate the properties of an antimicrobial surfactant-like peptide $(Ala)_6(Arg)$, A_6R, containing a cationic headgroup. The interaction of this peptide with zwitterionic (DPPC) lipid vesicles is investigated using a range of microscopic, X-ray scattering, spectroscopic, and calorimetric methods. The β-sheet structure adopted by A_6R is disrupted in the presence of DPPC. A strong effect on the small-angle X-ray scattering profile is observed: the Bragg peaks from the DPPC bilayers in the vesicle walls are eliminated in the presence of A_6R and only bilayer form factor peaks are observed. All of these observations point to the interaction of A_6R with DPPC bilayers. These studies provide insight into interactions between a model cationic peptide and vesicles, relevant to understanding the action of antimicrobial peptides on lipid membranes. Notably, peptide A_6R exhibits antimicrobial activity without membrane lysis.
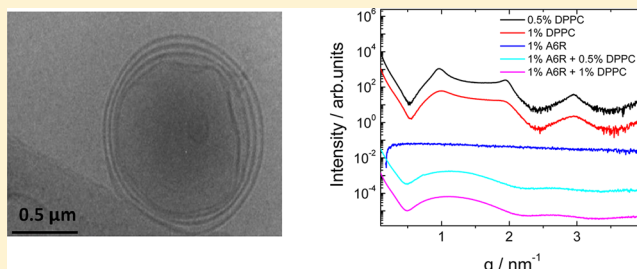
INTRODUCTION

Surfactant-like peptides (SLPs) have a remarkable ability to self-assemble into different nanostructures, primarily due to their amphiphilic nature. For example, they can aggregate into high aspect ratio structures while displaying bioactive peptides. SLPs are a class of amphiphilic peptide comprising a headgroup which is a short sequence of charged residues attached to a tailgroup of neutral residues.[1,2] Pioneering work on SLPs has been conducted by the Zhang group including A_6D, V_6D, V_6D_2 and L_6D_2.[3,4] We have recently investigated the self-assembly of a cationic peptide which consists of six consecutive hydrophobic alanine residues as a tailgroup with a cationic arginine headgroup.[5] We reported that this SLP can self-assemble into ultrathin sheets at low concentrations and at higher concentrations the sheets wrap around to form nanotubes and helical ribbons.

Peptides rich in arginine are known to have antimicrobial activities.[6−9] An example includes the transcription activating peptide, TAT [transactivator of transcription] from HIV-1, which has been reported to have antimicrobial properties.[10,11] The TAT peptide is 11 amino acids long, and it is highly basic as it contains six arginine and two lysine residues. It was found that substitution of any of the basic residues with a neutral amino acid causes a reduction of antimicrobial activity, which arises from its ability to bind to cell membranes.[9] Arginine contains a guanidinium group which adopts a planar Y-shape, which can delocalize the cationic charge. As a result arginine can form bidentate hydrogen bonds with phosphates in lipid headgroups as well as electrostatic interactions. As arginine interacts with cell membranes, this can lead to negative curvature and subsequently to cell leakage giving rise to antimicrobial properties.[9,10,12]

Our group previously investigated the self-assembly of a peptide amphiphile (PA) hexadecyl-β-alanine-histidine (C_{16}-βAH) along with mixtures of multilamellar DPPC vesicles.[13] We observed that the PA self-assembles into nanotapes based on lamellae, that is, stacked bilayers. Mixing the PA with DPPC caused a transition from multilamellar to unilamellar vesicles. Moshe et al. have studied the interactions of a designer cell-penetrating peptide (CPP) with phospholipids including DOPC and DOPE.[14] The peptide consisted of an arginine residue with two short hydrophobic moieties either side to create hydrophobic and electrostatic interactions. At low concentrations, below the critical aggregation concentration, the peptide was reported to insert in the lipid bilayers and cause a reduction in the membrane thickness. The CPP was found to change the charge of the DOPC membrane and even cause a phase transition in DOPE from an inverted hexagonal to a multilamellar phase. These observations were ascribed to a change in the delicate balance of the hydrophobic, electrostatic interactions and steric effects.

Yaghmur et al. examined the effect of both anionic (A_6D) and cationic (A_6K) SLP's on the bicontinuous cubic phase ($Pn\overline{3}m$) of mono-olein.[15] At low concentrations of A_6D, a bicontinuous cubic structure is retained, and only at high concentrations of the peptide a phase transition to an inverted hexagonal phase occurs. The addition of A_6K to mono-olein had no effect on the phase transition. These observations were attributed to the ability of A_6D to fully penetrate the membrane interface in contrast to A_6K which essentially does not penetrate the membrane due to electrostatic repulsion. As A_6D is inserted, destabilization of the lipid bilayer occurs, leading to negative curvature in the membrane interface. Previously, our group studied the influence of anionic and nonionic surfactants (sodium dodecyl sulfate[16] and Pluronic P123,[17] respectively) on the self-assembly of a collagen stimulating PA, C_{16}-KTTKS. The PA is known to self-assemble into extended nanotapes in solution.[18] Both surfactants influenced the self-assembly of C_{16}-KTTKS since morphological transitions from nanotapes to fibrils were observed.

Here we report on the antimicrobial properties of A_6R. Then we attempt to understand by investigating the effect of the cationic peptide A_6R on the structure of model zwitterionic lipid (DPPC) vesicles using a combination of microscopic, spectroscopic, and scattering techniques. DPPC vesicles were selected as a model system, building on previous work in our group on lipopeptide/vesicle interactions.[19] Actually, DPPC is a suitable model for mammalian cell membranes, but not bacterial membranes.[20] Other mixtures containing zwitterionic lipids have been used to model eukaryotic membranes.[14,21] Bacterial membranes are typically rich in anionic lipids such as POPG (oleoyl-1-palmitoyl-*sn*-glycero-3-phosphoglycerol) or DPPG (1,2-dipalmitoyl-*sn*-glycero-3-phosphoglycerol).[20,22,23] The self-assembly of A_6R has been thoroughly characterized by us previously.[5] It is therefore of practical as well as fundamental interest to characterize the peptide−lipid interactions to further enhance our understanding of the mechanism of binding and to improve the development of antimicrobial applications for the future.

■ EXPERIMENTAL SECTION

Materials. Peptide NH_2-AAAAAAR-COOH, referred to as A_6R, was custom synthesized by CS Bio Company (Menlo Park, CA) and was received as the TFA salt variant. The purity was 97.01% by HPLC in water/acetonitrile (0.1% TFA). Electrospray-ionization mass spectroscopy (ESI-MS) indicated a molar mass 600.87 g mol^{-1} (600.69 g mol^{-1}, expected).

Control peptide A_6D was purchased from CS Bio. Purity was 99.87% by HPLC in water/acetonitrile (0.1% TFA). ESI-MS indicated a molar mass 559.33 g mol^{-1} (559.59 g mol^{-1}, expected).

The phospholipid, 1,2-dipalmitoyl-*sn*-glycero-3-phosphocholine, DPPC, was purchased from Sigma Aldrich, and has a molecular weight of 734.05 g mol^{-1}.

Bacterial Strains and Growth Media. *Escherichia coli* O157 strain BW25113, the parent strain of the Keio collection, was kindly provided by Professor H. Mori, Keio University, Japan. *Staphylococcus aureus* NCDO 949 was originally from the collection of the National Institute for Research in Dairying, now listed as NCIMB 13062. Strains were maintained as frozen stocks at −70 °C on Cryobeads (Prolab Diagnostics, Neston, U.K.), which were plated onto nutrient agar (NA, Oxoid) and incubated at 37 °C overnight (16−18 h) to obtain single colonies before storage at 4 °C. Experimental cultures were prepared by inoculating a single colony into 10 mL of tryptone soy broth (TSB) supplemented with 0.3% (w/v) yeast extract (TSBY), and incubating statically for 6 h at 37 °C. This culture was then subcultured into a fresh broth of TSB and incubated with shaking at 180 rev min^{-1} overnight at 37 °C before use. Viability was assessed by diluting samples in Maximum Recovery Diluent (MRD, Oxoid), and plating 0.02 mL volumes onto nutrient agar. Plates were incubated at 37 °C, and colonies were counted after 48 h. Colony counts were calculated by colony forming units (CFU) equal to number of colonies times dilution factor times volume (CFU = $N \times$ dilution factor $\times V$).

Preparation of Cell Suspensions. Cells were harvested by centrifugation at 1300 rpm, 5 °C, for 5 min. The pellet was resuspended in 1.5 mL of ice-cold phosphate-buffered saline (PBS, pH 7.0, Sigma-Aldrich), and 20 μL of this solution was diluted into 200 μL of peptide solution (5, 2.5, 1, 0.5 mg/mL) to give approximately 10^7 cells mL^{-1}. Control solutions were achieved by adding no peptide solution but MRD instead. These solutions were vortexed for 3 s and left for set time intervals (10, 20, 30, 40, 50, 60 min) before diluting with MRD and plating. Plates were then incubated at 37 °C overnight for 18−24 h, followed by a cell count (CFU calculation).

Sample Preparation. *Vesicle Preparation.* DPPC vesicles were prepared by the thin layer hydration method to ensure the formation of multilayered vesicles.[24] A measured quantity of DPPC was dissolved in ethanol and placed into a 100 mL round-bottom flask. The solvent was evaporated by using a rotary evaporator, which formed a thin DPPC film at the bottom of the flask. A measured quantity of water was added to the flask to make up the defined concentration. The flask was returned to the rotary evaporator, which was rotated while at 50 °C by submerging it under a water bath. The solution was then vortexed at 50 °C for approximately 5 min.

Solution Mixture Preparation. Solutions of 0.5, 1, and 2 wt % DPPC vesicles were first prepared followed by the addition of 1 wt % A_6R. A measured quantity of A_6R powder was added to a solution of DPPC vesicles to make up the three different solutions with different proportions of DPPC. The mixture was left to sonicate for 30 min at 50 °C to dissolve A_6R. Then the solution was left to equilibrate at room temperature for a few days before any measurements.

Cryogenic-Transmission Electron Microscopy (Cryo-TEM). Imaging was carried out using a field emission cryo-electron microscope (JEOL JEM-3200FSC), operating at 200 kV. Images were taken in bright field mode and using zero loss energy filtering (omega type) with a slit width of 20 eV. Micrographs were recorded using a Gatan Ultrascan 4000 CCD camera. The specimen temperature was maintained at −187 °C during the imaging. Vitrified specimens were prepared using an automated FEI Vitrobot device using Quantifoil 3.5/1 holey carbon copper grids with a hole size of 3.5 μm. Just prior to use, grids were plasma cleaned using a Gatan Solarus 9500 plasma cleaner and then transferred into an environmental chamber of a FEI Vitrobot at room temperature and 100% humidity. Thereafter, 3 mL of sample solution was applied on the grid and it was blotted twice for 5 s and then vitrified in a 1/1 mixture of liquid ethane and propane at temperature of −180 °C. The grids with vitrified sample solution were maintained at liquid nitrogen temperature and then cryo-transferred to the microscope.

X-ray Diffraction (XRD). Measurements were performed on stalks prepared by drying filaments of solutions containing 1 wt % A_6R mixed with 0.5, 1, and 2 wt % DPPC. Solutions of the mixtures were suspended between the ends of wax-coated capillaries and dried. The stalks were mounted (vertically) onto the four axis goniometer of a RAXIS IV++ X-ray diffractometer (Rigaku) equipped with a rotating anode generator. The sample−detector distance varied between 90 and 100 mm depending on the sample. The X-ray wavelength was λ = 1.54 Å. The wavenumber scale ($q = 4\pi \sin \theta/\lambda$, where 2θ is the scattering angle) was geometrically calculated using the size of each pixel in the detector screen (0.0898 mm) and the sample−detector distance. The XRD data was collected using a Saturn 992 CCD camera.

Small-Angle and X-ray Scattering (SAXS). Solution SAXS data was performed on the bioSAXS beamline BM29 at the ESRF, Grenoble, France. Solutions containing 1 wt % A_6R and 1 wt % A_6R mixed with 0.5, 1, and 2 wt % DPPC were loaded in PCR tubes in an automated sample changer. SAXS data was collected using a Pilatus 1 M detector. The sample−detector distance was 2.84 m. The X-ray wavelength was 0.99 Å.

Circular Dichroism (CD). Spectra were obtained using a Chirascan spectropolarimeter (Applied Photophysics, UK). CD was performed on solution mixtures containing DPPC vesicles with A_6R added later, with a 0.5 nm step, 1 nm bandwidth and 1 s collection time per step at 20 °C. Data with absorbance $A < 2$ only are presented. Measurements were repeated four times. Smoothing of the data was carried out using the supplied Chirascan software.

Isothermal Titration Calorimetry (ITC). ITC experiments were carried out using an iTC_{200} microcalorimeter from MicroCal Inc. The working cell was filled with 200 μL of 0.1 wt % DPPC solution (dissolved in water) and the reference cell was filled with deionized water. The titrant syringe was filled with a solution of 1 wt % A_6R. The ITC experiment was programmed to run 20 injections of 2 μL volume of the titrant solution (1 wt % A_6R) into the working cell (0.1 wt % DPPC) with 300 s lag between each injection to ensure return to the baseline. The syringe was stirred throughout the experiment at 500 rpm and the working cell was set at 25 °C. The data was analyzed using Origin 7 (MicroCal) by fitting the curve using the one set of sites model.

■ RESULTS

Since many antimicrobial peptides contain arginine residues,[8,9,25,26] it is of interest to investigate the antimicrobial activity of model arginine-containing peptides such as A_6R. The antibacterial activity of this peptide was assayed against Gram positive *S. aureus* and Gram negative *E. coli*. Against *S. aureus* in particular, peptide A_6R shows a significant time-dependent reduction in the number of colony-forming units as shown in Figure 1, in contrast to the control (culture medium only). At
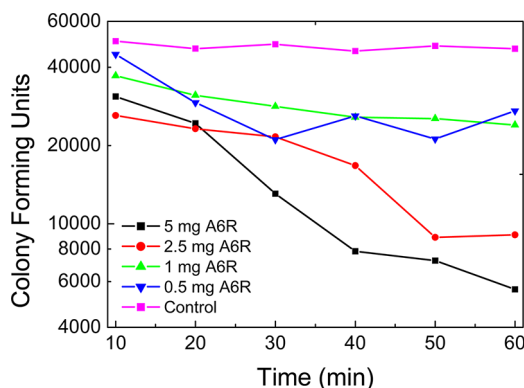
Figure 1. Antimicrobial testing results for A_6R with *S. aureus*. Dose and time dependence of colony forming units.

the highest peptide concentration used (5 mg/mL), a reduction in the number of colony-forming bacteria to approximately 15–25% of their initial number was observed after 1 h, with the reduction being larger the higher the peptide concentration. At the higher peptide concentration, the reduction is also greater for *S. aureus* than for *E. coli* (data shown in Supporting Information (SI) Figure 1a). As an additional control, the same protocol was followed but using peptide A_6D. Despite having an anionic (aspartic acid) headgroup rather than a cationic one, this peptide does exhibit some antibacterial activity (SI Figure 1b,c), although greatly reduced compared to A_6R. Peptide A_6D also showed greater activity against *S. aureus* than *E. coli*. The antibacterial activity of A_6R is larger than the reported 35-45% reduction in number of bacteria (*E. coli* or *S. aureus*) for A_6K to 55–65% surviving bacteria, although this peptide was studied only at lower concentration (up to 0.2 mg/mL).[27] Peptide A_9K showed better activity, in particular a reduction by 80% in

numbers of *E. coli* and 70% of *S. aureus* after 1 h for an 0.1 mg/mL sample.[27]

Having established the antimicrobial properties of A_6R, we set out to examine the origin of this effect in terms of interactions between the peptide and model lipid membranes, using DPPC vesicles. To investigate the binding interactions of A_6R with DPPC, CD spectroscopy was employed, along with other methods to be described shortly. Figure 2 presents CD
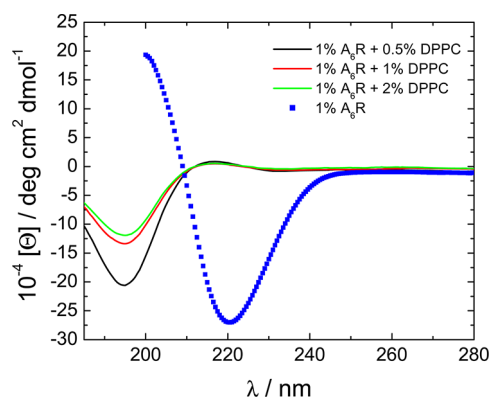
Figure 2. CD spectra of solutions of 1 wt % A_6R mixed with varying concentrations of DPPC compared with 1 wt % A_6R on its own.

spectra for 1 wt % A_6R on its own and with mixtures of 0.5, 1, and 2 wt % DPPC. The spectra show that A_6R adopts a β-sheet structure as a minimum at approximately 220 nm is observed.[28] This is consistent with our previous fiber XRD data, which revealed a β-sheet spacing.[5] Mixing of DPPC vesicles with A_6R leads to a spectrum indicative of a polyproline II (PPII) helix. The presence of a broad maximum band at ~220 nm due to $\pi_0 \rightarrow \pi^*$ (parallel electronic transition) and a minimum between 190 and 200 nm arising from the $\pi_0 \rightarrow \pi^*$ (perpendicular electronic transition) is characteristic of a PPII helix.[29] Detailed modeling of the change in peptide conformation on binding to the DPPC bilayer is beyond the scope of the present Article; however, it may be mentioned that many surface-active peptides undergo conformational changes upon binding to lipid membranes, for example, as well as antimicrobial peptides,[7] this has been very well studied for the amyloid β peptide.[30] It is clear that the CD spectrum from the mixture is completely different from that of A_6R on its own and cannot be expressed as a superposition of the spectra from the species in the mixture, which indicates interactions between the peptide and lipid vesicles.

Cryo-TEM images from solutions of 0.5, 1, and 2 wt % DPPC vesicles are shown in Figure 3a–c, respectively. The images reveal a variation in the size of the vesicles. The size of the vesicles varies greatly from approximately 150 nm to 2 μm or more. It was observed that smaller vesicles were often found inside larger vesicles. Sheets of DPPC not forming vesicles were also observed in the 0.5 wt % DPPC sample. As the concentration of DPPC increases from 0.5 to 1 wt %, a reduction in the number of sheets not forming vesicles was noted as well as a decrease in the fraction of larger vesicles. Upon addition of A_6R to a solution of DPPC, the multiwall vesicle structure is retained as shown in Figure 3d–f. For low DPPC concentration, the overall size of the vesicles largely remains the same as those of DPPC vesicles in the absence of A_6R; however, the size distribution of vesicles shifted toward smaller particles for 1 wt % A_6R + 2 wt % DPPC. Notably, the
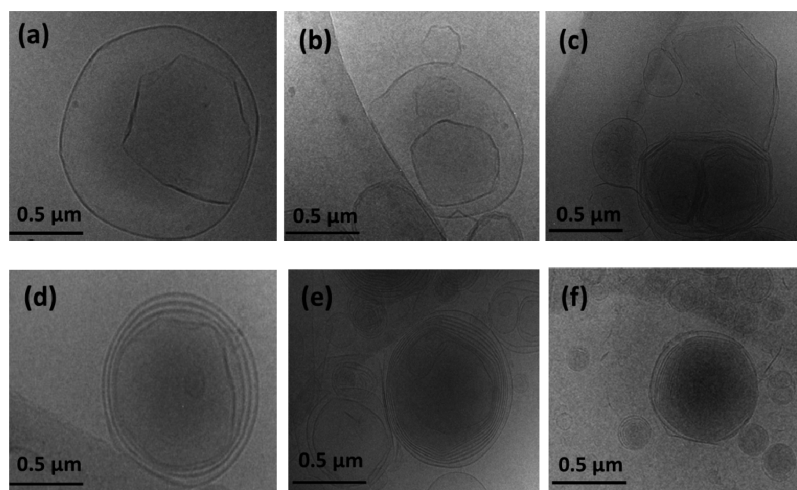
Figure 3. Cryo-TEM images of DPPC vesicles of varying concentrations containing (a) 0.5 wt %, (b) 1 wt %, and (c) 2 wt %. Images of 1 wt % A_6R solution mixed with (d) 0.5 wt % DPPC, (e) 1 wt % DPPC, and (f) 2 wt % DPPC.

addition of A_6R does not cause membrane disruption and break up of vesicles.

Microscopy can provide valuable information; however, to provide nonlocal information on the average nanostructure, SAXS was employed to compliment the cryo-TEM images and to further elucidate the influence of A_6R on the structure of the DPPC walls. SAXS intensity profiles for A_6R/DPPC mixtures are plotted along with their individual components for comparison as shown in Figure 4. The data for 1 wt% A_6R
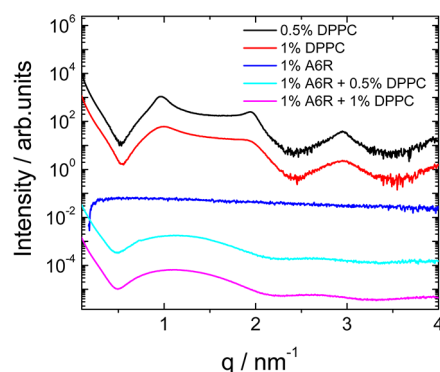

Figure 4. SAXS one-dimensional profiles comparing the different ratio mixtures of 1 wt % A_6R with DPPC vesicles and its individual components. The SAXS curves have been shifted to enable visualization of the data.

has been presented before and reveals the self-assembly of the peptide into flat sheet-like nanostructures.[5] The DPPC phospholipid vesicles were prepared by using the rehydration method to ensure the development of multilamellar vesicles.[24]

The SAXS curves for 0.5 wt %, 1 wt % and 2 wt % DPPC contain of structure factor peaks, which are due to a stacking arrangement within the multilamellar walls. A periodicity of 64.8 Å was obtained from the highest order of diffraction for both 0.5 wt % and 1 wt % DPPC, which is in good agreement with previous literature.[31−36] A contribution of a bilayer form factor as well as structure factor due to the stacking arrangement of the DPPC walls is present and therefore was taken into consideration when fitting the SAXS intensity profile for DPPC using the modeling software, SASfit.[37] A fit to a model comprising a Gaussian bilayer form factor along with a

modified Caillé structure factor (described in our previous work[13]) for 1 wt % DPPC is presented in Figure 5a, and the
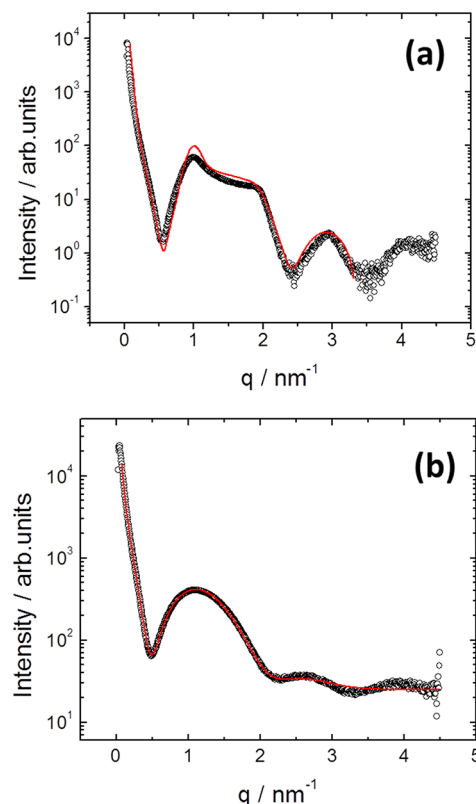

Figure 5. SAXS profiles for (a) 1 wt % DPPC fitted to a Gaussian bilayer form factor along with a modified Caillé structure factor and (b) 1 wt % A_6R + 1 wt % DPPC fitted to a Gaussian bilayer form factor.

fitting parameters are listed in Table 1. A fit to the SAXS profile for 0.5 wt % DPPC is shown in SI Figure 2. The SAXS curves for the mixtures are well fitted to a Gaussian bilayer form factor excluding the modified Caillé structure factor since the structure factor peaks are no longer present.

SAXS confirms a multilamellar architecture for DPPC in the vesicle walls with a period of 64.8 Å. This value is too small to

Table 1. Parameters for Fits to SAXS Data Shown in Figure 5 and SI Figure 2 Determined from SASfit

sample	σ_{out}	b_{out}	σ_{core}	b_{core}	N	d [Å]	η
0.5 wt % DPPC	0.09	0.01	0.59	−0.002	4	63.6	0.15
1 wt % DPPC	0.09	0.01	0.54	−0.002	3	63.6	0.25
1 wt % A_6R + 0.5% DPPC	0.10	0.02	1.04	−0.002			
1 wt % A_6R + 1% DPPC	0.57	0.01	1.80	−0.005			

observe the stacking arrangement within the vesicle walls using cryo-TEM. As A_6R is inserted in the bilayers, cryo-TEM suggests the retention of multilamellar vesicles, which are noticeable in Figure 3. However, the SAXS structure factor peaks are lost (Figure 5b and SI Figure 2b). This indicates that the local multilamellar order is disrupted, possibly due to swelling effects (cryo-TEM shows multilayer vesicles with a vesicle wall spacing much larger than 6.5 nm). The profound change in SAXS intensity profiles, suggests that A_6R has inserted in the lipid bilayers. Since DPPC is zwitterionic it is likely that A_6R interacts with the negative charge on the phosphate group favoring insertion into the bilayer.

Fiber XRD stalks dried from solution were employed to obtain further structural detail in the wider angle regions. Representative XRD patterns are shown in SI Figure 3. Equatorial and meridional XRD intensity profiles for 1 wt % DPPC and 1 wt % A_6R mixed with 1 wt % DPPC are shown in Figure 6. The one-dimensional intensity profile for 1 wt %
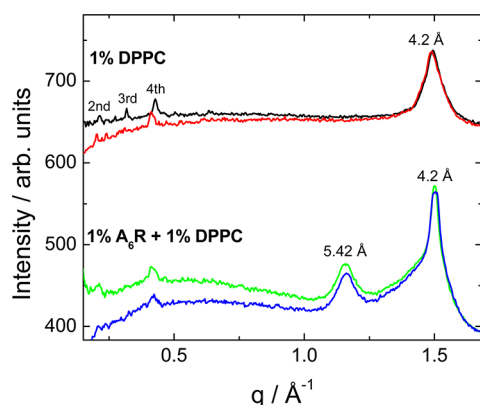

Figure 6. XRD one-dimensional radial profiles (equatorial and meridional radial averages) for 1 wt % DPPC and 1 wt % A_6R + 1 wt % DPPC with indicated *d*-spacings. The XRD curves have been shifted to enable visualization of the data. Line colors: 1% DPPC, black = equatorial and red = meridional; 1% A_6R + 1% DPPC, green = equatorial and blue = meridional.

DPPC exhibits several peaks corresponding to second, third and fourth order reflections associated with the multilayer structure of DPPC, which can be observed especially for a 2 wt % sample as shown in SI Figure 4c. In addition, a peak with a *d*-spacing of 4.2 Å can also be observed. This peak has been previously reported for DPPC, and was ascribed to the hexagonal packing of the fatty acid side chains of phospholipid.[38,39] The 4.2 Å lipid chain spacing is still present upon the addition of A_6R to DPPC in 1:1 (Figure 6), 1:0.5 and 1:2 (SI Figure 4) mixtures. An additional 5.42 Å reflection was also observed for the mixtures. Recently we reported a 5.5 Å spacing for dilute concentrations (0.5% - 4%) of A_6R, which was assigned to the polyalanine β-sheet spacing.[5] This suggests

that some β-sheet like ordering is retained, possibly due to the presence of a population of DPPC-free A_6R sheets or due to the presence of "rafts" of ordered A_6R within the DPPC vesicle walls. However, circular dichroism spectroscopy (Figure 1) indicates the absence of a significant β-sheet content globally in the system under the same conditions.

To further probe the possible interactions between A_6R and DPPC we employed isothermal titration calorimetry. ITC is a well-known technique to enable investigation of the molecular interactions of biological samples, in this case a peptide-lipid interaction. A solution of 1 wt % A_6R was injected into 0.1 wt % DPPC since A_6R is the ligand and DPPC acts as the receptor. A low concentration of DPPC was selected for ITC to reduce the total number of binding sites to ensure saturation of A_6R binding to DPPC was reached. The ITC profile for the titration of A_6R into DPPC is presented in Figure 7, which exhibits a
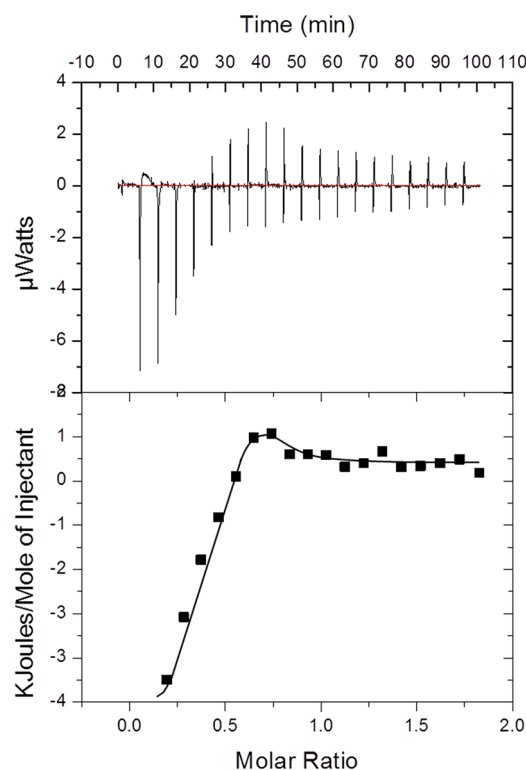

Figure 7. ITC profile for 1 wt % A_6R solution injected into a solution of 0.1 wt % DPPC.

series of negative peaks, indicating an exothermic reaction. The integration and normalization of the exothermic peaks produced a sigmoidal curve relative to the moles of ligand added, which was then appropriately fitted to a one set of sites model. The one set of sites model was used for the peptide/lipid system as it is assumed that each binding site has the same binding affinity. A binding constant $K = 1.25 \times 10^5$ M^{-1} was determined from the fitting parameters. Other parameters including the number of binding sites $N = 0.3$, enthalpy $\Delta H = -3817$ J mol^{-1} and entropy $\Delta S = 4.84$ J mol^{-1} K^{-1} were also obtained from the fit.

Previous studies have examined binding in peptide/lipid mixtures. Domingues et al. investigated the binding of an 18 amino acid long antimicrobial peptide interacting with charged large unilamellar vesicles (LUVs).[40] They reported that the binding of the peptide to LUVs is mainly an exothermic

process. The binding of a cationic pentapeptide composed of analogs of lysine resides to negatively charged phospholipid, DPPG was investigated.[41] It was reported that an exothermic reaction occurs upon binding. A binding constant, $K = 5.4 \times 10^5$ M^{-1}, was determined, which is a similar value to the one we obtained. The Vogel group also investigated the binding of an antimicrobial peptide, Ac-FRWWHR-NH$_2$ to POPG vesicles, which reveal an exothermic reaction and a binding constant, $K = 3.13 \times 10^5$ M^{-1}.[42] The mentioned examples are in good agreement with our observations that an exothermic process occurs during binding and the binding constant values are similar to those we obtained.

■ SUMMARY AND DISCUSSION

In summary, A$_6$R interacts with DPPC vesicles leading to changes in the vesicle wall layer spacing such that the SAXS structure factor peaks present for DPPC vesicles are eliminated and only the form factor of isolated bilayers is observed. This is similar to what is observed for the interaction of the peptide amphiphile C$_{16}$-βAH (βAH: β-alanine-histidine dipeptide, known as L-carnosine) with DPPC.[13] X-ray diffraction indicates the presence of a fraction of tightly packed alanine-rich β-sheet structures in the A$_6$R/DPPC mixtures, although circular dichroism spectroscopy shows the suppression of global β-sheet ordering of A$_6$R in the presence of DPPC. Some A$_6$R may form separate β-sheet assemblies or "rafts" of ordered A$_6$R may be present in the vesicle walls. Discriminating between these possibilities is a challenge for future work.

Interestingly, A$_6$R does not seem to permeabilize DPPC vesicles despite its insertion into the vesicle walls (as inferred from dramatic changes in the SAXS intensity profiles). Addition of the peptide leads to the loss of structure factor peaks. This is the opposite of the behavior observed by Moshe et al. for their GFfWG (f: D-phenylalanine) peptide interacting with model cell membranes (DOPS, DOPC, DOPE mixture) since a series of Bragg reflections were observed in the presence of the peptide, but only form factor (similar to that shown in our Figure 4b) features were observed for the membrane/lipid mixture.[14]

Hoernke et al. reported that short basic pentapeptides such as K$_5$ insert into lipid (DPPG) membranes,[41] in contrast to the findings of Ben-Tal et al.[43] However, in neither of these studies was imaging of vesicles or permeabilization measurements performed. The hexapeptide FRWWHR, identified by combinatorial screening methods to have strong antimicrobial activity, does not cause substantial leakage from vesicles, and Rezansoff et al. suggested that the bactericidal action of the peptide may involve translocation across the membrane.[42] However, Blondelle et al. did observe lysis of model DPPC-containing membranes in the presence of lysine-rich 18-mer peptides.[44] Natural antimicrobial peptides such as magainin[45,46] and gomesin[40] permeabilize membranes and lead to lysis. Some cationic peptides are known to cause fusion of cell membranes and have been studied in particular in the context of viral infection where they mediate fusion of the host cell membrane and the enveloped virus. The fusogenic TAT protein transduction domain has been used to deliver a wide range of biologically active cargo (DNA, proteins, liposomes, and others).[47] The initial model for cellular uptake involves direct penetration across the lipid membrane, however it has been shown that TAT-fusion proteins are rapidly internalized by lipid-raft dependent macropinocytosis[47] (pinocytosis is non-specific endocytosis within vesicles). As mentioned above,

substitution of any of the basic residues in the TAT peptide with a neutral amino acid causes a reduction of antimicrobial activity, reflecting the influence of charge and hydrophobicity.[9]

Thus, prior work indicates that membrane permeabilization can occur for peptides with more than one cationic residue, but this alone is not sufficient. The sequence and length of the peptide is also important, as is the nature and composition of the lipid membrane. This was highlighted by Chen et al. in their comparison of the antibacterial properties of A$_3$K, A$_6$K, and A$_9$K.[27] They found that the latter, which has the longest hydrophobic alanine block and the strongest aggregation tendency, has the highest antimicrobial activity. This peptide also did not significantly disrupt DPPC vesicles, although DPPG membranes were broken up. Even relatively short peptides righ in arginine and/or tryptophan have potent antimicrobial activity.[26] Other factors influencing the activity of antimicrobial peptides are discussed elsewhere.[48] As discussed in the Introduction, models for bacterial cell membranes should consist of anionic lipids although as discussed above many studies have used DPPC as model membranes.

We have shown that A$_6$R is a model antimicrobial cationic peptide containing a single arginine residue attached to a hydrophobic hexa-alanine sequence to drive self-assembly. This study provides insight into its interaction with model lipid membranes. It also introduces the concept of addition of SLPs to modulate the structure of lipid vesicles. Remarkably, A$_6$R exhibits antimicrobial activity without zwitterionic lipid membrane lysis.

■ ASSOCIATED CONTENT

ⓈSupporting Information

Antimicrobial activity data for control peptide A6D, additional SAXS and XRD data. This material is available free of charge via the Internet at http://pubs.acs.org.

■ AUTHOR INFORMATION

Notes

The authors declare no competing financial interest.

■ ACKNOWLEDGMENTS

■ REFERENCES

(1) Hamley, I. W. Self-Assembly of Amphiphilic Peptides. *Soft Matter* **2011**, *7*, 4122.

(2) Zhao, X.; Pan, F.; Xu, H.; Yaseen, M.; Shan, H.; Hauser, C. A.; Zhang, S.; Lu, J. R. Molecular Self-Assembly and Applications of Designer Peptide Amphiphiles. *Chem. Soc. Rev.* **2010**, *39*, 3480.

(3) Vauthey, S.; Santoso, S.; Gong, H.; Watson, N.; Zhang, S. Molecular Self-Assembly of Surfactant-Like Peptides to Form Nanotubes and Nanovesicles. *Proc. Natl. Acad. Sci. U.S.A.* **2002**, *99*, 5355.

(4) Maltzahn, G. V.; Vauthey, S.; Santoso, S.; Zhang, S. Positively Charged Surfactant-Like Peptides Self-Assemble into Nanostructures. *Langmuir* **2003**, *19*, 4332.

(5) Hamley, I. W.; Dehsorkhi, A.; Castelletto, V. Self-Assembled Arginine-Coated Peptide Nanosheets in Water. *Chem. Commun.* **2013**, *49*, 1850.

(6) Nicolas, P.; Mor, A. Peptides as Weapons against Microorganisms in the Chemical Defense System of Vertebrates. *Annu. Rev. Microbiol.* **1995**, *49*, 277.

(7) Chan, D. I.; Prenner, E. J.; Vogel, H. J. Tryptophan- and Arginine-Rich Antimicrobial Peptides: Structures and Mechanisms of Action. *Biochim. Biophys. Acta, Biomembr.* **2006**, *1758*, 1184.

(8) Reddy, K. V.; Yedery, R. D.; Aranha, C. Antimicrobial Peptides: Premises and Promises. *Int. J. Antimicrob. Agents* **2004**, *24*, 536.

(9) Schmidt, N.; Mishra, A.; Lai, G. H.; Wong, G. C. Arginine-Rich Cell-Penetrating Peptides. *FEBS Lett.* **2010**, *584*, 1806.

(10) Mishra, A.; Lai, G. H.; Schmidt, N. W.; Sun, V. Z.; Rodriguez, A. R.; Tong, R.; Tang, L.; Cheng, J. J.; Deming, T. J.; Kamei, D. T.; Wong, G. C. L. Translocation of HIV TAT Peptide and Analogues Induced by Multiplexed Membrane and Cytoskeletal Interactions. *Proc. Natl. Acad. Sci. U.S.A.* **2011**, *108*, 16883.

(11) Piantavigna, S.; McCubbin, G. A.; Boehnke, S.; Graham, B.; Spiccia, L.; Martin, L. L. A Mechanistic Investigation of Cell-Penetrating TAT Peptides with Supported Lipid Membranes. *Biochim. Biophys. Acta* **2011**, *1808*, 1811.

(12) Zhao, K.; Choe, U.-J.; Kamei, D. T.; Wong, G. C. L. Enhanced Activity of Cyclic Transporter Sequences Driven by Phase Behavior of Peptide−Lipid Complexes. *Soft Matter* **2012**, *8*, 6430.

(13) Castelletto, V.; Cheng, G.; Stain, C.; Connon, C. J.; Hamley, I. W. Self-Assembly of a Peptide Amphiphile Containing L-Carnosine and Its Mixtures with a Multilamellar Vesicle Forming Lipid. *Langmuir* **2012**, *28*, 11599.

(14) Moshe, L.; Saper, G.; Szekely, O.; Linde, Y.; Gilon, C.; Harries, D.; Raviv, U. Modulating the Structure and Interactions of Lipid−Peptide Complexes by Varying Membrane Composition and Solution Conditions. *Soft Matter* **2013**, *9*, 7117.

(15) Yaghmur, A.; Laggner, P.; Zhang, S.; Rappolt, M. Tuning Curvature and Stability of Monoolein Bilayers by Designer Lipid-Like Peptide Surfactants. *PLoS One* **2007**, e479.

(16) Castelletto, V.; Hamley, I. W.; Adamcik, J.; Mezzenga, R.; Gummel, J. Modulating Self-Assembly of a Nanotape-Forming Peptide Amphiphile with an Oppositely Charged Surfactant. *Soft Matter* **2012**, *8*, 217.

(17) Dehsorkhi, A.; Castelletto, V.; Hamley, I. W.; Lindner, P. Influence of a Non-Ionic Amphiphilic Copolymer on the Self-Assembly of a Peptide Amphiphile That Forms Nanotapes. *Soft Matter* **2012**, *8*, 8608.

(18) Castelletto, V.; Hamley, I. W.; Perez, J.; Abezgauz, L.; Danino, D. Fibrillar Superstructure from Extended Nanotapes Formed by a Collagen-Stimulating Peptide. *Chem. Commun.* **2010**, *46*, 9185.

(19) Castelletto, V.; Cheng, G.; Stain, C.; Connon, C. J.; Hamley, I. W. Self-Assembly of a Peptide Amphiphile Containing L-Carnosine and Its Mixtures with a Multilamellar Vesicle Forming Lipid. *Langmuir* **2012**, *28*, 11599.

(20) Hu, J.; Chen, C. X.; Zhang, S. Z.; Zhao, X. C.; Xu, H.; Zhao, X. B.; Lu, J. R. Designed Antimicrobial and Antitumor Peptides with High Selectivity. *Biomacromolecules* **2011**, *12*, 3839.

(21) Zhao, K.; Choe, U. J.; Kamei, D. T.; Wong, G. C. L. Enhanced Activity of Cyclic Transporter Sequences Driven by Phase Behavior of Peptide-Lipid Complexes. *Soft Matter* **2012**, *8*, 6430.

(22) Domingues, F. S.; Riske, K. A.; Miranda, A. Revealing the Lytic Mechanism of the Antimicrobial Peptide Gomesin by Observing Giant Unilamellar Vesicles. *Langmuir* **2010**, *26*, 11077.

(23) Taheri-Araghi, S.; Ha, B. Y. Cationic Antimicrobial Peptides: A Physical Basis for Their Selective Membrane-Disrupting Activity. *Soft Matter* **2010**, *6*, 1933.

(24) Szoka, F.; Papahadjopoulos, D. Procedure for Preparation of Liposomes with Large Internal Aqueous Space and High Capture by Reverse-Phase Evaporation. *Proc. Natl. Acad. Sci. U.S.A.* **1978**, *75*, 4184.

(25) Nicolas, P.; Mor, A. Peptides as Weapons. *Annu. Rev. Microbiol.* **1995**, *49*, 277.

(26) Chan, D. I.; Prenner, E. J.; Vogel, H. J. Tryptophan- and Arginine-Rich Antimicrobial Peptides: Structures and Mechanisms of Action. *Biochim. Biophys. Acta* **2006**, 1758−1184.

(27) Chen, C. X.; Pan, F.; Zhang, S. Z.; Hu, J.; Cao, M. W.; Wang, J.; Xu, H.; Zhao, X. B.; Lu, J. R. Antibacterial Activities of Short Designer Peptides: A Link between Propensity for Nanostructuring and Capacity for Membrane Destabilization. *Biomacromolecules* **2010**, *11*, 402.

(28) Woody, R. W. *Circular Dichroism of Peptides and Proteins*; New York, 1994.

(29) Wallace, B. A.; Janes, R. W. Synchrotron Radiation Circular Dichroism Spectroscopy of Proteins: Secondary Structure, Fold Recognition and Structural Genomics. *Curr. Opin. Chem. Biol.* **2001**, *5*, 567.

(30) Hamley, I. W. The Amyloid Beta Peptide: A Chemist's Perspective. Role in Alzheimer's and Fibrillization. *Chem. Rev.* **2012**, *112*, 5147.

(31) Tristram-Nagle, S.; Zhang, R.; Suter, R. M.; Worthington, C. R.; Sun, W. J.; Nagle, J. F. Measurement of Chain Tilt Angle in Fully Hydrated Bilayers of Gel Phase Lecithins. *Biophys. J.* **1993**, *64*, 1097.

(32) McManus, J. J.; Radler, J. O.; Dawson, K. A. Phase Behavior of Dppc in a DNA-Calcium-Zwitterionic Lipid Complex Studied by Small-Angle X-Ray Scattering. *Langmuir* **2003**, *19*, 9630.

(33) Sun, W. J.; Tristram-Nagle, S.; Suter, R. M.; Nagle, J. F. Structure of Gel Phase Saturated Lecithin Bilayers: Temperature and Chain Length Dependence. *Biophys. J.* **1996**, *71*, 885.

(34) Tenchov, B. G.; Yao, H.; Hatta, I. Time-Resolved X-Ray Diffraction and Calorimetric Studies at Low Scan Rates. *Biophys. J.* **1989**, *56*, 757.

(35) Hauet, N.; Artzner, F.; Boucher, F.; Grabielle-Madelmont, C.; Cloutier, I.; Keller, G.; Lesieur, P.; Durand, D.; Paternostre, M. Interaction between Artificial Membranes and Enflurane, a General Volatile Anesthetic: DPPC-Enflurane Interaction. *Biophys. J.* **2003**, *84*, 3123.

(36) Quinn, P. J.; Takahashi, H.; Hatta, I. Characterization of Complexes Formed in Fully Hydrated Dispersions of Dipalmitoyl Derivatives of Phosphatidylcholine and Diacylglycerol. *Biophys. J.* **1995**, *68*, 1374.

(37) http://kur.web.psi.ch/sans1/SANSSoft/sasfit.html, in 2013.

(38) Mckersie, B. D.; Thompson, J. E. Influence of Plant Sterols on the Phase Properties of Phospholipid Bilayers. *Plant Physiol.* **1979**, *63*, 802.

(39) Katsaras, J.; Yang, D. S.-C.; Epand, R. M. Fatty-Acid Chain Tilt Angles and Directions in Dipalmitoyl Phosphatidylcholine Bilayers. *Biophys. J.* **1992**, *63*, 1170.

(40) Domingues, T. M.; Mattei, B.; Seelig, J.; Perez, K. R.; Miranda, A.; Riske, K. A. Interaction of the Antimicrobial Peptide Gomesin with Model Membranes: A Calorimetric Study. *Langmuir* **2013**, *29*, 8609.

(41) Hoernke, M.; Schwieger, C.; Kerth, A.; Blume, A. Binding of Cationic Pentapeptides with Modified Side Chain Lengths to Negatively Charged Lipid Membranes: Complex Interplay of Electrostatic and Hydrophobic Interactions. *Biochim. Biophys. Acta* **2012**, *1818*, 1663.

(42) Rezansoff, A. J.; Hunter, H. N.; Jing, W.; Park, I. Y.; Kim, S. C.; Vogel, H. J. Interactions of the Antimicrobial Peptide Ac-FRWWHR-NH₂ with Model Membrane Systems and Bacterial Cells. *J. Pept. Sci.* **2005**, *65*, 491.

(43) Ben-Tal, N.; Honig, B.; Peitzsch, R. M.; Denisov, G.; McLaughlin, S. Binding of Small Basic Peptides to Membranes Containing Acidic Lipids: Theoretical Models and Experimental Results. *Biophys. J.* **1996**, *71*, 561.

(44) Blondelle, S. E.; Takahashi, E.; Houghten, R. A.; Perez-Payá, E. Rapid Identification of Compounds Having Enhanced Antimicrobial Activity Using Conformationally Defined Combinatorial Libraries. *Biochem. J.* **1996**, *313*, 141.

(45) Matsuzaki, K.; Sugishita, K.; Ishibe, N.; Ueha, M.; Nakata, S.; Miyajima, K.; Epand, R. M. Relationship of Membrane Curvature to the Formation of Pores by Magainin 2. *Biochemistry* **1998**, *37*, 11856.

(46) Papo, N.; Shai, Y. Exploring Peptide Membrane Interaction Using Surface Plasmon Resonance: Differentiation between Pore Formation Versus Membrane Disruption by Lytic Peptides. *Biochemistry* **2003**, *42*, 458.

(47) Wadia, J. S.; Stan, R. V.; Dowdy, S. F. Transducible Tat-Ha Fusogenic Peptide Enhances Escape of TAT-Fusion Proteins after Lipid Raft Macropinocytosis. *Nature* **2004**, *10*, 310.

(48) Brogden, K. A. Antimicrobial Peptides: Pore Formers or Metabolic Inhibitors in Bacteria? *Nat. Rev. Microbiol.* **2005**, 3, 238.